Report No. LR-614

The Application of the Finite Element Method to an Aerodynamic Problem Specific to Propeller Design

March 1990

Cyril M. Wentzel

TU Delft
Delft University of Technology

Faculty of Aerospace Engineering

The Application of the Finite Element Method to an Aerodynamic Problem Specific to Propeller Design

Cyril M. Wentzel

Summary

For the solution of a classical problem occuring in propeller aerodynamics: finding the optimum circulation distribution (minimum energy loss in the wake), a finite element method has been applied and programmed.

In doing so, no specific numerical problems were encountered and the method has been verified (linear elements) using classical tables in the literature.

The program yields an efficient and flexible means of generating the optimum distribution for open propellers of arbitrary bladenumber and for any advance coefficient.

In addition to this, the applicability of this finite element model to ducted propeller theory is explored.

CONTENTS

LIST OF SYMBOLS

B	Number of blades
ω	Angular velocity of propeller
V	Free stream velocity (advance velocity for propeller)
w	Displacement velocity (virtual, axial)
V_3	$= V+w$
ψ	Local sheet pitch angle
x,y,z	Carthesian coordinates
r,z,θ	Cylindrical coordinates
μ,ξ,η	Curvilinear helicoïdal coordinates
i,j,k	Unit vectors in r,θ,z directions
x,y	Conveniently scaled coordinates for computational domain $(\mu\lambda_3,\xi)$
λ_3	Velocity ratio in final wake $[= V_3/\omega r]$
λ_i	$i = 1,2,3$ Linear supportfunctions corresponding to nodes i
Φ_i	$i = 1,2,3,12,23,31$ Quadratic functions corresponding to nodes i
ϕ	(Velocity-) Potential
ϕ	Supportfunction for approximation of the solution
$\bar{\phi}$	Nondimensionalised potential; $= \phi/[V_3 w/\omega]$
$K(x)$	Circulation coefficient $= B\bar{\phi}/\pi$
Ω	Indicating a surface (area)
$\partial\Omega$	Boundary of area

SECTION 1

INTRODUCTION

In the theory of propeller aerodynamics there appears a problem of finding a suitable distribution of thrust along the radius of the propeller. One way of solving this problem is to assume a rigid vortex-sheet far down in the slipstream. This rigid vortex sheet, if it could exist at all, can be proven to represent minimum induced losses (kinetic energy) for a given thrust. It must be mentioned that the resulting circulation distribution, appearing in this context of a designpoint calculation, is also used in so-called strip analysis methods for general off-design conditions.

The solution for this problem can be established by finding the potential jump across the vortex sheet, since this is directly related to the circulation distribution along the lifting line representation of the propeller blade. Thus we are interested in the potential at the sheet surface. This sheet appears to be moving (axially) downstream at a velocity w, the so-called displacement velocity, and the sheet's geometry is helicoidal. It determines the boundary condition for a potential flow where the flow far away of the slipstream is undisturbed (i.e. at rest). This situation is illustrated in fig.1.

A potential flow is governed by the Laplace equation for the velocity potential. Also, it is of paramount importance to note that the present problem (i.e. boundary condition) is axisymmetric and periodic; the three dimensional formulation can therefore be reduced to a two-dimensional one.

This modified mathematical problem can be solved analytically using Bessel functions as presented by Goldstein in his classical paper, ref.1. It is, however, restricted to application to 2- and 4-bladed propellers. This was then extended to an arbitrary number of blades by Lock (ref.2), using semi-empirical extrapolation techniques, based on Prandtl's method (yielding results which suffice for technical purposes): Prandtl's approximation yields a solution in closed form via a two dimensional analogy and complex transformations, and gives exact results in the limit of zero pitch angle for the system of helicoidal sheets. Using another exact solution for infinite pitch, a trend is established

over the whole range of blade numbers, and the magnitude of the solution is adjusted according to the two solutions of Goldstein. The results of this procedure are extensively used in the form of tables.

Goldstein's analytical approach itself is complex indeed, and for a non-specialist probably difficult to understand mathematically. Also, a need is felt to check the solutions and the extrapolations made by Lock. Therefore, and to make a solution more flexible to arbitrary boundary conditions, numerical methods can be used.

One such numerical approach was adopted by Morrison (ref.3) by using finite difference methods. It quickly gives good results, but can in two respects be considered not to be elegant: first, the Neumann boundary conditions at the sheet boundary prompt for the usual interpolation techniques (though these are alleviated by the symmetry that is typical of this problem) and second, the difficulties of locally refining the grid are prohibitive.

A second numerical approach will be elaborated in the present work: The finite element method (FEM) will be applied to the two dimensional Laplace equation using linear elements. Chapter 2 will present the theory, to be followed by a section which will use its results to develop the system of simultaneous equations (Chapter 3). A computer program, dedicated to the present computational problem, was developed and is discussed in Section 4.
Test runs, comparisons and the conclusions then conclude this report in Section 5 and 6.

The results in section 5 reveal a secondary purpose pursued by developing this FEM application: In par. 5.5 an the present model is placed in the context of ducted propeller design, and an exploration is made identifying the theoretical refinements that need to be made to result in a design method which would be the equivalent of the classical approach to the design of optimum open propellers.

SECTION 2

THEORY

2.1 The governing equations

The equation that governs potential flow is the Laplace equation. Because of the nature of the problem, cylinder coordinates are used; in these coordinates (r,θ,z), the Laplace equation for the potential ϕ is:

$$\nabla^2\phi = \frac{\partial^2\phi}{\partial r^2} + \frac{1}{r}\frac{\partial\phi}{\partial r} + \frac{1}{r^2}\frac{\partial^2\phi}{\partial\theta^2} + \frac{\partial^2\phi}{\partial z^2} = 0 \qquad (2.1)$$

The boundary for computational purposes can be concentrated around the smallest entity: we will call this a unit cell. At first sight (fig.2) it appears to be bounded by:

- the z-axis,
- two consecutive vortex sheets,
- the extension of these sheets,
- the area at infinite radius.

At closer inspection, however, it follows from symmetry conditions (anti-symmetry within cell with boundaries as described above) that there is a helicoidal plane in the middle of two helicoidal vortex sheets on which the potential can be put equal to zero (antisymmetry). Computationally, we will therefore restrict the unit cell to half the cell as described before. This area is schematically indicated in fig.2.

The boundary conditions on the sheets stem from the axial velocity of the helicoidal sheets, as illustrated in fig.3. From this:

$$w\cos\psi = \frac{\partial\phi}{\partial z}\cos\psi - \frac{1}{r}\frac{\partial\phi}{\partial\theta}\sin\psi \qquad (2.2)$$

Also, because of undisturbed flow far away from the body, the boundary at infinity has zero potential:

$$\phi = 0, \qquad r \to \infty \tag{2.3}$$

From symmetry considerations it follows that there cannot be a radially induced velocity component at (actually, within) one of the vortex sheets, nor at the helicoidal plane that extends from it. Combined with (2.3) this must mean that on these extended sheets the potential equals zero since the gradient along the radial direction is zero there:

$$\phi = 0, \quad r > R, \quad \theta = \frac{2\pi}{B} n, \quad n = 1,2,\ldots., B \tag{2.4}$$

where B is the number of blades.
Finally, there is an obvious Neumann boundary condition of zero flow through the z-axis:

$$\frac{\partial \phi}{\partial n} = \frac{\partial \phi}{\partial r} = 0, \qquad r = 0 \tag{2.5}$$

It is useful to rewrite the first Neumann condition to become:

$$w = \frac{\partial \phi}{\partial z} - \frac{1}{r} \frac{V_3}{\omega r} \frac{\partial \phi}{\partial \theta} \tag{2.6}$$

since for the local pitch angle, ψ: $\tan \psi = \frac{V+w}{\omega r} = \frac{V_3}{\omega r}$
V_3, as introduced at this place, refers to an apparent relative axial velocity (for an observer attached to the propeller) determining the pitch of the system; it consists of the forward velocity V and the displacement velocity w.

2.2 Transformation to two dimensions

From symmetry and periodicity considerations it follows that there is no change of solution (potential) along the direction of a helicoidal surface. In consequence, a new curvilinear coordinate system with one coordinate in this direction and the other pointing away from such a surface, will bring about the desired two dimensional formulation of the problem. These coordinates can easily be found by recalling that the equation which describes a helicoidal sheet, the pitch of which is determined by ω (angular velocity) and V_3 ("forward velocity"), is:

$$\theta - \frac{\omega z}{V_3} = \text{constant}$$

Now the set of coordinates (μ,ξ,η) is introduced by

$$\left.\begin{aligned} \mu &= \frac{\omega r}{V_3} = \frac{r/R}{\lambda_3} \\ \xi &= \theta - \frac{\omega z}{V_3} \\ \eta &= \theta + \frac{\omega z}{V_3} \end{aligned}\right\} \quad (2.7)$$

The differential operators that are to be substituted then become (using $\partial/\partial\eta=0$ for the specific part of the solution we are interested in):

$$\left.\begin{aligned} \frac{\partial}{\partial r} &= \frac{\omega}{V_3}\frac{\partial}{\partial \mu} \quad ; \quad \frac{\partial^2}{\partial r^2} = \frac{\omega^2}{V_3^2}\frac{\partial^2}{\partial \mu^2} \\ \frac{\partial}{\partial z} &= -\frac{\omega}{V_3}\frac{\partial}{\partial \xi} \quad ; \quad \frac{\partial^2}{\partial z^2} = \frac{\omega^2}{V_3^2}\frac{\partial^2}{\partial \xi^2} \\ \frac{\partial}{\partial \theta} &= \frac{\partial}{\partial \xi} \quad ; \quad \frac{\partial^2}{\partial \theta^2} = \frac{\partial^2}{\partial \xi^2} \quad ; \quad \frac{1}{r} = \frac{\omega}{\mu V_3}, \ \frac{1}{r^2} = \frac{\omega^2}{\mu^2 V_3^2} \end{aligned}\right\} \quad (2.8)$$

(It should be noted that the exact form of the 3rd equation of 2.7 is not required)

The Laplace equation then transforms to

$$(\frac{\omega}{V_3})^2 . \left[\frac{\partial^2 \phi}{\partial \mu^2} + \frac{1}{\mu} \frac{\partial \phi}{\partial \mu} + \frac{1+\mu^2}{\mu^2} \frac{\partial^2 \phi}{\partial \xi^2} \right] = 0 \qquad (2.9)$$

Finally, the boundary conditions must be adapted, which involves only a reformulation of (2.6) yielding:

$$w = - \frac{\omega}{V_3} \left(\frac{1+\mu^2}{\mu^2}\right) \frac{\partial \phi}{\partial \xi} \qquad (2.10)$$

In the next paragraph the scaling factors pertaining to the definition (2.7) of the new coordinates u_i are required for integration and differentiation purposes. These scaling factors, which specify an increment of (Cartesian) length ds to be related to du_i by $ds=h_i.du_i$, follow directly from its definition:

$$h_i = \left| \frac{\partial \underline{r}}{\partial u_i} \right|$$

For the Cartesian positionvector r we have, expressed in cylindrical coordinates:

$$\underline{r} = r.\cos\theta \, \underline{i} + r.\sin\theta \, \underline{j} + z\underline{k}$$

Partial differentiation now yields:

$$\frac{\partial \underline{r}}{\partial \xi} = \frac{\partial \underline{r}}{\partial r} \cdot \frac{\partial \underline{r}}{\partial \xi} + \frac{\partial \underline{r}}{\partial \theta} \cdot \frac{1}{\partial \xi / \partial \theta} + \frac{\partial \underline{r}}{\partial z} \cdot \frac{1}{\partial \xi / \partial z}$$

$$= 0 + (-r.\sin\theta \, \underline{i} + r.\cos\theta \, \underline{j}) - \frac{V_3}{\omega} \underline{k}$$

Taking the norm of this vector we get for the scaling factor h_ξ:

$$h_\xi = \left| \frac{\partial \underline{r}}{\partial \xi} \right| = \sqrt{r^2 + (\frac{V_3}{\omega})^2} = \frac{V_3}{\omega} \sqrt{\frac{\mu}{1 + \mu^2}}$$

In an analogous manner we find:

$$h_\mu = \frac{V_3}{\omega}$$

And because μ and ξ are orthogonal we can form the Jacobian from the scaling factors. A surface integral in Cartesian coordinates transforms to a surface integral in μ,ξ with the Jacobian:

$$J = h_\xi . h_\mu = \left(\frac{V_3}{\omega}\right)^2 \sqrt{\frac{\mu}{1+\mu^2}}$$

$$\longrightarrow \int_\Omega \{int\} d\Omega = \int_\Omega \{int\} \left(\frac{V_3}{\omega}\right)^2 \sqrt{\frac{\mu}{1+\mu^2}}\, d\mu\, d\xi \qquad (2.10a)$$

2.3 Order reduction

If equation (2.9) holds at any point in the domain, then also the integrated function (over an area Ω), after multiplication with a 'testfunction' v, should be identically zero; making use of (2.10a) we obtain:

$$\int_\Omega v \left\{\frac{\partial^2\phi}{\partial\mu^2} + \frac{1}{\mu}\frac{\partial\phi}{\partial\mu} + \left(\frac{1+\mu^2}{\mu^2}\right)\frac{\partial^2\phi}{\partial\xi^2}\right\} \sqrt{\frac{\mu}{1+\mu^2}}\, d\xi\, d\mu = 0 \qquad (2.11)$$

If (2.9) represents the "strong" formulation for the differential equation, then the integrated form (2.11) is generally known as a "weak" formulation, in this case of our Laplace problem.

We rewrite (2.11) with the vector identity

$$v\, \nabla . A = -\nabla v . A + \nabla . (vA)$$

where $A=\nabla\phi$, into the form

$$\iint \nabla v . \nabla\phi = \iint \nabla . (v\nabla\phi)$$

Now, applying Green's theorem to the RHS yields

$$\iint \nabla v . \nabla\phi \, d\Omega = \oint v \frac{\partial\phi}{\partial n}\, ds$$

Rewriting the area integral in terms of the new coordinates then yields

$$\int_{\Omega} \left\{ v_{\mu}\phi_{\mu} + \frac{1+\mu^2}{\mu^2} v_{\xi}\phi_{\xi} \right\} \frac{\mu}{\sqrt{1+\mu^2}} \, d\xi d\mu = \int_{\partial\Omega} v \frac{\partial\phi}{\partial n} \, ds \qquad (2.16)$$

The derivatives in this equation are of the first order each. The surface integral will be developed to result in a system of equations of which the line integral will form the right hand side. This will be done in the next section.

2.4 Application of Ritz approximation and Galerkin's method

In order to discretise the problem, the solution for the potential will be approximated by piecewise multivariate polynomials. The span of each of these polynomials will (in the next section) be made equal to the size of the surface elements into which the domain will be divided. Each of these polynomials is then characterised by a finite number of coefficients. These coefficients then become the unknowns (i.e. the local solution for the potential) of the problem. This approach is called the Ritz method, viz:

$$\bar{\phi}(\mu,\xi) = \sum_{i=1}^{n} u_i \, \phi_i(\mu,\xi) \qquad (2.17)$$

Here the potential is divided by a constant c_1, derived from the parameters in the problem. From this point on we nondimensionalize both sides of the governing equation by this constant c_1 according to:

$$\bar{\phi} = \frac{\phi}{c_1} \; ; \quad c_1 = \frac{V_3 w}{\omega} \qquad (2.18)$$

Please note that for typographical reasons the notation for the potential and for the support functions are the same (ϕ).
Before the integral can be evaluated it is also necessary to make a choice for the testfunctions. According to the Galerkin-method it is chosen to be identical to the supporting functions in (2.17).

$$v_j = \phi_j \, (\mu,\xi)$$

In developing the equations further it is practical to use the set of scaled coordinates according to:

$$x = \mu\lambda_3 \;;\quad dx = \lambda_3\, d\mu$$
$$y = \xi \;;\quad dy = d\xi \tag{2.19}$$

where x extends in the radial direction from the root (x=0) to the tip (x=1) and further to infinity.
At this point the boundary conditions can be taken into account to establish the second part of (2.15). The boundary $\partial\Omega$ consists of three parts (fig. 4).
At $\partial\Omega_3$ equations (2.3) and (2.4) state that the solution be identically zero. In the finite element approach we typically set the test functions v (i.e. ϕ_j) equal to zero at points j where an essential boundary condition applies. In this way the corresponding equations disappear from the problem.
Next, the natural boundary condition at the left (inner) boundary makes the integral vanish at $\partial\Omega_1$.
All that remains is the integral at $\partial\Omega_2$, i.e. the vortex sheet. Here, the normal derivative is (positive outwards of Ω):

$$\left(\frac{\partial\phi}{\partial n}\right)_{\partial\Omega_2} = -\frac{1}{h_\xi}\frac{\partial\phi}{\partial\xi} = -\frac{\omega}{V_3}\left(\frac{\sqrt{1+\mu^2}}{\mu}\right)\cdot\frac{\partial\phi}{\partial\xi}$$

On the other hand, we have from the boundary condition (2.10):

$$\frac{\partial\phi}{\partial\xi} = -\frac{wV_3}{\omega}\left(\frac{\mu^2}{1+\mu^2}\right)$$

from which

$$\left(\frac{\partial\phi}{\partial n}\right)_{\partial\Omega_2} = \frac{\omega}{V_3}\frac{\mu}{\sqrt{1+\mu^2}}$$

and, also for ds we have

$$ds = \frac{V_3}{\omega}\, d\mu$$

Now the line integral becomes:

$$\int_{\partial\Omega} \phi_j \frac{\partial\phi}{\partial n}\, ds = \frac{1}{\lambda_3} \int_{\partial\Omega_2} \phi_j \frac{x}{\sqrt{x^2+\lambda_3^2}}\, dx$$

The resulting equation for fixed j then emerges after moving the summation of (2.17) and the unknowns u_i outside the integral of (2.16):

$$\sum_{i=1}^{n} u_i \left\{ \int_{\Omega} \phi_{j_x} \phi_{i_x} f(x) + \phi_{j_y} \phi_{i_y} g(x)\, dxdy \right\} = \int_{\partial\Omega_2} \phi_j f(x)\, dx \qquad (2.20)$$

where $f(x) = \frac{x}{\sqrt{x^2+\lambda_3^2}} \cdot \lambda_3^2$

and $g(x) = \sqrt{x^2+\lambda_3^2}\ /x$

This result can serve as a starting point for developing the system of equations, which become apparent after recalling that this equation should hold for every testfunction v, so for every ϕ_j. There belongs one testfunction to every one supporting point (node) of an element, which results in as many equations as there are unknowns.

SECTION 3

DEVELOPING THE SYSTEM OF SIMULTANEOUS EQUATIONS

The total system of simultaneous equations consists of one equation per node. The corresponding matrix of coefficients will be termed the 'big matrix'; for every one entry of this matrix there are several contributing elements of the computational mesh. Such a contribution of an element we will then call an 'element matrix'; it will be further elaborated in par.3.3.

3.1 The linear element

In order to perform the integrations the solution is to be approximated by piecewise polynomials. The span of these polynomials extends over a part of the domain, called an element. In this paragraph a particular choice for this polynomial will be made to be a linear function (of two variables), selected for its illustrative simplicity.

The linear approximation over an element consists of the sum of three separate functions λ_i, i=1,2,3. Each of these belongs to one of the corresponding nodes (unknowns) of the triangular element; at this corresponding node the basisfunction is identically one while the others vanish (fig.5).
We will denote this linear basisfunction by λ, in spite of the same notation adopted for the velocity ratio (i.e. λ_3). In order to evaluate the surface integral of (2.20), we need to find an expression for the derivatives of the approximation to the solution in both directions. Assuming λ to be of the form:

$$\lambda = c_0 + c_1 x + c_2 y \qquad (3.1)$$

, we therefore have to establish the coefficients c_1 and c_2. These follow from

the three interpolation conditions which e.g. determine λ_1 :

$$\lambda_1(x_1) = 1$$

$$\lambda_1(x_2) = 0 \qquad (3.2)$$

$$\lambda_1(x_3) = 0$$

Now, using Cramer's rule, c_1 and c_2 become:

$$c_1 = \frac{y_2 - y_3}{D} \quad ; \quad c_2 = \frac{x_3 - x_2}{D} \qquad (3.3)$$

In these expressions, D is the determinant, for which:

$$D = x_1 (y_2 - y_3) + x_2 (y_3 - y_1) + x_3 (y_1 - y_2) \qquad (3.4)$$

The two other support functions (belonging to the other vertices) follow simply by cyclic perturbation of the indices.

3.2 The quadratic element

A more accurate polynomial to approximate the solution, in two dimensions characterised by six support functions and six nodes (see fig.5), is the polynomial of second degree, Φ_i. It is most conveniently expressed in terms of the linear support functions λ_i, defined in the preceding paragraph.

Here, we have six interpolation conditions, where as an example Φ_3 equals 1 at x_3 and vanishes at the other five points $x_{3,1}..x_{2,3}$. By looking at these conditions "with a carpenter's eye", we can immediately conclude that Φ_3 can only be a function of λ_3 and that there is no constant term involved, which makes the template:

$$\Phi_3 = a\lambda_3 + b\lambda_3^2 \qquad (3.5)$$

Interpolating at x_3 and vanishing at x_{31} then results in:

$$\Phi_3 = \lambda_3(2\lambda_3 - 1) \tag{3.6}$$

As a template for the second kind of quadratic function we then consider Φ_{12}, which is identically 1 at x_{12}, vanishes at the other points and can on second glance only be a function of λ_1 and λ_2. Only one condition is necessary to determine Φ_{12} as:

$$\Phi_{12} = 4\lambda_1\lambda_2 \tag{3.7}$$

The other functions Φ_i follow from the corresponding template by adjusting the indices occurring within it.

Finally, we also need expressions to evaluate the derivatives. It is easily verified that:

$$\partial\Phi_3/\partial x = (4\lambda_3 - 1)\,\lambda_{3_x} \tag{3.8}$$

$$\partial\Phi_{12}/\partial x = 4(\lambda_1\lambda_{2_x} + \lambda_2\lambda_{1_x}) \tag{3.9}$$

The derivatives of the linear function, λ_{i_x} were already established in the previous paragraph as the coefficients c_1 and c_2.

3.3 The element matrix

In order to compute the big matrix the following approach, typical of finite element methods is used: the elements are scanned successively and their individual contributions are added to the corresponding positions in the big matrix. Thus, we typically consider the small matrix, also called the element matrix. We denote it by S^e_{ij}. According to the generic equation (2.20), it consists of two parts: S^e_{ijI} and S^e_{ijII}. Because of the nature of the problem, the element matrix is symmetrical.

The element matrix for the linear elements has a size 3x3 and the quadratic element involves a 6x6 matrix. This last matrix can be divided into four 3x3 parts, three of which are themselves essentially different.

Out of the nine elements of a **linear** 3x3 (sub-)matrix, there are only two essentially different elements, i.e. the rest follows from one template by adjusting the indices that occur in the expressions in a cyclic manner. Thus, we discern S^e_{11} and S^e_{12} to be typical for a linear element.

The quadratic sub-matrices, however, feature more essentially different elements, which are even not that easily identified. In the next paragraph expressions for these will be developed; also, the templates will be used in the computer program.

For the integration over the element e either Newton-Côtes or Gaussian integration can be used. The much simpler Newton-Côtes method is generally considered to be adequate up to second degree elements. In the next paragraphs the linear and the quadratic element matrix will be developed for the present problem, involving the Newton-Côtes integration rule and two and seven generic matrix elements respectively.

3.3.1. The linear element matrix

After substitution of the expressions for the derivatives, (3.3), the integral to be solved (2.20) becomes:

$$\int_e c_{1_j}\, c_{1_i}\, f(x)\, dx\, dy + \int_e c_{2_j}\, c_{2_i}\, g(x)\, dx\, dy \qquad (3.10)$$

Newton-Côtes integration means an approximation of the integrand by polynomials of the same degree as the support functions that occur in it. In this linear case the integral for S^e_{11} then works out as follows:

$$\int_e \text{int}\,(x)\, dx\, dy \approx \frac{|D|}{6}\left[\text{int}\,(x_1) + \text{int}\,(x_2) + \text{int}\,(x_3)\right] \qquad (3.11)$$

$$\rightarrow S^e_{11} = \frac{(y_2-y_3)^2}{6|D|}\{f(x)_1+f(x)_2+f(x)_3\} + \frac{(x_3-x_2)^2}{6|D|}\{g(x_1)+g(x_2)+g(x_3)\} \quad (3.12)$$

Likewise, substitution and successive integration yields for the template S^e_{12} for S_{ij}, $j \neq i$:

$$S^e_{12} = \frac{(y_2-y_3)(y_3-y_1)}{6|D|}\{f(x_1)+f(x_2)+f(x_3)\}$$

$$+ \frac{(x_3-x_2)(x_1-x_3)}{6|D|}\{g(x_1)+g(x_2)+g(x_3)\} \quad (3.13)$$

The expression for the determinant was already given in (3.4), representing twice the area of the element-triangle.

3.3.2. The quadratic element matrix

Only the results of making the necessary substitutions are presented here. The Newton-Côtes expression in R^2, corresponding to the quadratic element, is the so-called 3-point formula:

$$\int_e \text{int}(\mathbf{x})\, d\Omega \approx \frac{|D|}{6}\{\text{int}(\mathbf{x}_{12}) + \text{int}(\mathbf{x}_{23}) + \text{int}(\mathbf{x}_{31})\} \quad (3.14)$$

Utilising equations (3.8) & (3.9) for the quadratic functions and keeping in mind the linear functionvalues (1/2) at these particular support (mid-)points, we can now determine this sum for all the elements of the 6x6 matrix in turn. Schematically, the element matrix is comprised of parts A, B and D as follows:

$$\begin{vmatrix} A & B \\ B & D \end{vmatrix}$$

For brevity, we will consider only the first part of the total integral, with the understanding that both contributions should be summed, substituting the correct function for the function f(x) and substituting the slopes a_i (b_i) of the linear functions λ_i, i.e:

$$a_i = c_1 |D|$$
$$b_i = c_2 |D| \qquad (3.15)$$

For the diagonal blocks A and D we thus have,

$$S^e_{1,1}{}_I = \frac{a_1^2}{6|D|}\{f(x_{12}) + f(x_{23}) + f(x_{31})\}$$

$$S^e_{1,2}{}_I = \frac{a_1 a_2}{6|D|}\{f(x_{12}) - f(x_{23}) - f(x_{31})\} \qquad (3.16)$$

$$S^e_{12,12}{}_I = \frac{4}{6|D|}\{(a_1+a_2)^2 f(x_{12}) + a_1^2 f(x_{23}) + a_2^2 f(x_{31})\}$$

$$S^e_{12,23}{}_I = \frac{4}{6|D|}\{a_3(a_1+a_2)f(x_{12}) + a_1(a_2+a_3)f(x_{23}) + a_2^2 f(x_{31})\}$$

Now, for submatrix B, using one generic expression, though possibly sufficient, seems to become a bit messy, so three equations are presented (and programmed), one for each member of a row; these can then be perturbed in the positive diagonal direction to yield the other elements:

$$S^e_{1,12}{}_I = \frac{2a_1}{6|D|}\{(a_1+a_2)f(x_{12}) - a_1 f(x_{23}) + a_2 f(x_{31})\}$$

$$S^e_{1,23}{}_I = \frac{2a_1}{6|D|}\{a_3 f(x_{12}) - (a_2+a_3)f(x_{23}) + a_2 f(x_{31})\} \qquad (3.17)$$

$$S^e_{1,31}{}_I = \frac{2a_1}{6|D|}\{a_3 f(x_{12}) - a_1 f(x_{23}) + (a_1+a_3)f(x_{31})\}$$

3.4 The element vector

Equation (2.20) gives the line integral from which the right hand side of the system of simultaneous equations should follow after substitution of equations (3.1) and (3.5) respectively. Though it would be possible to approximate it by using Newton-Côtes, an exact evaluation is applied here, simply because the solution is exactly known.

In case of linear line elements the function λ_j to be substituted for ϕ_j is, e.g. for λ_1:

$$\lambda_1 = c1 + c2.x$$

where

$$c1 = -x_1/\ell \; ; \quad c2 = 1/\ell \; ; \quad \ell = x_2 - x_1$$

Multiplying with f(x) (see (2.20)), the integrand for the line integral consists of two parts, each resulting in standard integrals of the type:

$$\int \frac{x^m}{\sqrt{x^2+a^2}}\, dx \quad (=K_m)$$

The solutions for these standard integrals are presented here for m=1,2,3:

$$K_1 = \sqrt{x^2+a^2}$$
$$K_2 = 0.5\,\left[x\sqrt{x^2+a^2} - a^2 \ln(x+\sqrt{x^2+a^2})\right]$$
$$K_3 = \left[(x^2+a^2)^{3/2}\right]/3 - a^2\sqrt{x^2+a^2}$$

If we denote the line integrals from x_1 to x_2 involving K_q by I_q, then we get for the two members of the linear element vector $\mathbf{b}^e$:

$$b_1^e = -\,(-x_1 . I_1 + I_2)/\ell$$
$$b_2^e = \quad (-x_2 . I_1 - I_2)/\ell \qquad (3.18)$$

If **quadratic** elements are applied, then (3.6) and (3.7) represent the corresponding quadratic function on the basis of λ_1 (and λ_2) as given above.

The resulting polynomial $c1 + c2.x + c3.x^2$ for ϕ_1 then has the coefficients:

$$c1 = (x_1 + x_2)x_2/\ell^2$$
$$c2 = (x_1 + 3x^2)/\ell^2$$
$$c3 = 2/\ell^2$$

For Φ_2 these follow from correspondingly changing the indices.
For Φ_{12} we get:

$$c1 = 4x_1 x_2/\ell^2$$
$$c2 = 4(x_1 + x_2)/\ell^2$$
$$c3 = -4/\ell^2$$

With these coefficients and using the standard integrals the three components of the element vector become:

$$b_1^e = 1/\ell^2 \{ x_2(x_1 + x_2)I_1 + (x_1 + 3x_2)I_2 + 2I_3 \}$$

$$b_2^e = 1/\ell^2 \{ x_1(x_1 + x_2)I_1 + (3x_1 + x_2)I_2 + 2I_3 \} \qquad (3.19)$$

$$b_{12}^e = 4/\ell^2 \{ x_1 x_2 I_1 + (x_1 + x_2)I_2 - I_3 \}$$

SECTION 4

NUMERICAL ASPECTS

4.1 General set up of FEM-program OPT-CIRK

Because of the specific nature of the problem now under investigation, a dedicated computer program to solve it quickly for different parameters after effective experimentation with numerical parameters (i.e. the mesh) was thought to be useful. The current chapter presents the methods used for mesh generation, matrix manipulation and interaction with the user.

The program has been set up for use on an ATARI 1040-ST computer, making use of the 'WIMP interface' offered by GEM (Digital Research's "Graphical Environment Manager"), which is itself integrated into the computer's operating system. The machine has up to 1 Mb of internal memory, which turned out to be sufficient to cope with a fine mesh, provided that use was made of the banded character of the numerical problem. The FORTRAN compiler that was used (Prospero) is equiped with the necessary bindings to make use of GEM (also available for MSDOS-machines) and offers the Fortran-77 standard, augmented with some extensions (like mixed types in common blocks, type checking, long names and comments on the same line). The possibility of mixed language programming (with Pascal, especially useful for interactive applications) was not considered necessary for this limited application.

As a typical GEM application, the program as such features an 'event managed' structure and therefore needs no further explanation; the possible alternative actions open to the user (as determined by the state of the program) are at any time reflected in the drop-down menus (items of which are either enabled or disabled). Its features are:

* input by means of a dialog form on screen
* inspection of the mesh on screen
* calculating the solution
* contour plot on screen
* inspection of solution on vortex sheet
* numerical output of relevant part to printer

The program's numerical core consists of the following actions, to be performed sequentially, which are programmed in distinct procedures (though they are in fact FORTRAN subroutines).

{ precondition: problem specific- and mesh- parameters specified }
* Setting up the mesh
* Merging the boundary conditions into the numbering scheme
* Resetting the big matrix and vector
* Setting up the big matrix and the big vector
* Factorisation of matrix without pivotting
* Backward substitution to yield solution

4.2 Generating the mesh: numbering scheme

The functional domain has a rectangular shape, as can be seen from fig.4. The numerical mesh is depicted schematically in fig.6.
The choice of triangular elements is natural, applicable to both linear and quadratic elements.

The lower limit in x-direction can be set to some small non-zero value (0 corresponds to a singularity), while the upper limit is open to experimentation, but should be representative of infinity.
The 'blade-tip' region correponds to x=1.0, which is also the transition from Neumann to Dirichlet boundary conditions. The boundary conditions themselves are for clarity summarised in fig.4.

A large amount of effort could be put into trying to design a mesh generator that could generate a near-optimum layout of triangles. Rather than to do this,

a provision was made that would offer some control over the refinement of the mesh size in certain areas. Specifically, it can be expected that the area inside of the blade tip requires refinement, though formally also accuracy in the area of small radii could require refinement because of a strong change in curvature of the potential along the sheet (see the inflection point in fig.8). It was decided to offer this refinement in both directions, but for the 'horizontal' one in both the inner and outer region. The refinement can then be expressed as a ratio of the relevant length of the first and the last element of that area. From this value ('fact1' in the program) the multiplication factor (factor1) can be found from the following expression, given the interval length (length) and the number of elements (n_el):

```
factor1 = fact1**(1.0/(n_el-1))
```

The first step in this direction then has the length:

```
step1_x = length / POL(n_el,factor1)
```

where POL(..) is the functionvalue of a polynomial of degree n_el, having coefficients equal to 1, given an argument factor1.

An alternative to this method of refinement would be to use a Chebychev distribution of points on the inner region, giving refinements at both the outer (tip) and the inner (hub) parts where curvature of the solution is highest. This alternative, though simple to implement is not further applied in the present work.

Of course the node-numbering system is important here. It was expected that the y-direction would require the least elements for a given accuracy. Therefore it was decided to maintain a vertical direction for numbering (see fig.6). In this way the band-width of the big matrix is reduced to a minimum, which is important for storage.

The elements themselves are numbered in a horizontal direction in a straightforward manner, giving rise to two element types, I and II (with respect to the following).

In scanning the elements, determining the element matrices and assembling the big matrix, an expression is required that will relate element numbers to node-identity indices. The following was found to yield that information:

$$i = 1 + \{ (j-1)DIV(2*n\_el) + ((j-1)MOD(n\_el)+1)*(m+1) + ..$$

$$- ((j-1)DIV(n\_el))MOD(2)*m \} * stepmult$$

where stepmult is 1 in case of linear and 2 in case of quadratic elements and m is the number of small triangles (elements in the linear case and sub- elements in the quadratic case). Figure 6 also indicates for which node the index i is found to belong to an element j for both type I and II elements.

In the program, S/R 'fill' assigns x- and y-values to all the nodes in the mesh. After that, S/R 'vul_nodig' is called to scan the edges where an essential boundary condition applies, and an array 'strip_index' (originally a one-to-one copy of the index) is edited in such a way that an index k in the computational domain will correspond to (point to the same node as) ℓ = strip_index(k). Also, a boolean array 'nodig' is filled with flags indicating whether or not a node is part of the numerical domain.

4.3 Assembling the big matrix and big vector

In S/R 'vul_grote_matrix' each element is scanned in turn. A 'scan' involves determining the 3x3 or 6x6 element matrix according to the equations in par.3.3 (S/R 'elem' or 'elem2') and adding the members of that matrix to the corresponding positions in the big matrix (S/R 'plaats_el').

Here, the connection between element- and node-numbers mentioned in the preceding paragraph is applied in S/R 'Element_To_Index' which is called from S/R 'vul_grote_matrix'.

Before the functionality of 'plaats_el' is discussed, it should be mentioned that only (the upper) half of the big matrix, being symmetric because of the underlying Laplace operator, is stored and manipulated (see next paragraph).

Therefore, care must be taken in adding the contributions (i.e. elmat(i,j)) to the big matrix. If the node numbers of i and j would correspond to the lower triangle of the matrix, this must be accounted for by adding it to the corresponding position in the upper triangle.

In an analogous manner, but without any complications, S/R 'vul_vector' uses 'vector(_2)' and 'plaats_vec' to assemble the big vector according to the equations in par. 3.4.

4.4 Solving the system of simultaneous equations

The matrix of the system of simultaneous equations is numerically convenient and well behaved: It is symmetric, positive definite and banded.

As to the bandedness: if vertically, there are 'm' elements, then an arbitrary node in the inner region might 'reach' as far as m+1 (or 2*(m+1) for quadratic elements) to both sides as far as the influence of the corresponding support function is concerned (not m+1+1 because the upper horizontal boundary is essential). Therefore, the bandwidth is 1 + 2*(2*(m+1)) in the quadratic case, and because of symmetry only 1+(2*(m+1)) codiagonals need then to be stored.

Neither is more storage required for the manipulation (factorisation) of the matrix, because there is no need for pivotting (definitely positive).

For the solution of this system of (n*m - n_o) equations, the combination DPBFA and DPBSL from the subroutine library LINPACK was selected for the factorisation and backsubstitution respectively. The first requires the main diagonal and the upper codiagonals to be stored in the rows, and the columns of the upper triangle at the same time to be stored in the columns of the presented matrix. After factorisation, its output is used for backward substitution in a straightforward manner.

The translation from an arbitray position in the full matrix to the position in the reduced matrix is performed in S/R 'plaats_el', where also the aforementioned possible conversion to the upper half is done.

4.5 User interface of OPT-CIRK

A typical GEM-application features a drop-down menu for control, a window based environment for (graphical) output and so-called dialogs for interactive input /output. The so-called menubar of OPT_CIRK can be distinguished in the upper part of figure 9 to 11. An illustration of the selection of a sub-item of this menu can be found in figure 11b. The event management using such a menu set-up offers an immediate and ever-present possibility to modify the numerical or the problem's parameters, as well as to inspect the solution.

This data input is done by interacting with the dialog that is shown in fig.9, which in this case contains all the necessary settings, such as number of elements, refinement parameters, choice between linear and quadratic elements and also the two parameters determining the problem itself: the number of blades and the advance coefficient. The S/R 'Get_Parameters' takes care of the actions required for the input.

Before the computation is started, an immediate inspection of the resulting grid is possible by selecting 'Show Mesh' in the parameters menu (S/R 'Show_Mesh') as is illustrated in figure 10..

The computation itself is then invoked by selecting 'Go' from the 'Compute' menu and after a few seconds of resetting the contents of the matrix and vector, the user is informed about the progress of the elimination process by a (non-interactive) dialog showing the percentual progress (from the number of rows).

The solution for the potential is then multiplied by a certain value (obviously depending on the problem's two parameters) to yield values ('dimensionless circulation' K(x)) which are of direct use.

Finally, the results are open for inspection by selecting the 'Show Contourplot' item from the 'Output' menu which by now has been enabled. By default, an 'alert-box' appears inquiring whether or not the present contents of the window should be erased. This facility makes it possible to study certain effects in terms of observed changes in the contourlines. Additionally, the numerical maximum value of the solution appears in the window's info-line (fig.11a).

An additional facility to make a plot of the solution along the vortex sheet and compare different solutions w.r.t. each other as well as to a well known approximation (Prandlt) is also implemented (fig.11b&c), as is a facility to make a HPGL file for plotter output.

Because of the nature of the problem, the same big matrix cannot be used for different problem parameters (see equation (2.20), where λ_3 appears in the integral on the left hand side) so at every run a new matrix is assembled and factored.

A typical computation requires some 15 seconds for an accurate solution with linear elements (see discussions in next paragraphs), which is considered to be reasonable.

SECTION 5

DISCUSSION OF RESULTS

5.1 Comparison cases: Goldstein's and Prandtl's method

As was noticed in the introduction section, the exact solution for this boundary value problem is given by Goldstein's method. This will be taken here as a case for assessing the current solution's accuracy. Figure 8 is reproduced from ref.1; it gives the solution for two cases (two and four propeller blades) at relatively low advance ratio (0.2).

Goldstein also provides a table of 16 calculated values for the scaled circulation, up to 3 significant digits, which should make comparisons easier. If ϕ indicates the potential at the vortex sheet, then the results are expressed in terms of:

$$K(x) = \frac{B\Gamma\omega}{2\pi w V_3} = \frac{B\phi\omega}{\pi w V_3} \qquad (5.1)$$

A second case for comparison works the other way around: Prandtl's method gives an approximation, which is more accurate the lower the advance ratio and the higher the number of blades. An impression of its accuracy can be acquired from looking at the same figure (8), where dashed lines lie particularly close to the exact solution for the case of 4 blades. As soon as some confidence has been gained in the accuracy of the present method, it can be used to assess the accuracy of Prandtl's approximation over the whole range.
The mathematical expression for this approximation is:

$$K(x) = \frac{2}{\pi} \cdot \arccos e^{-f} \cdot \frac{x^2}{x^2 + \lambda_3^2}$$

$$f = \frac{B(1-x)}{2 \sin\psi} \qquad (5.2)$$

The data published by Goldstein in ref.1 are limited. For this reason comparison data were taken from Theodorsen (ref.4) who also summarises data taken from Kramer (ref.5). as well as Lock&Yeatman. Where appropriate, these data have been

interpolated by Theodorsen to yield values for even fractions. Thus, comparison data are available to verify the numerical approach over a whole range of advance coefficient, the results of which will be presented in paragraph 5.3

In the comparisons to be made it must be noted that the magnitude of the maximum circulation is particularly important since it determines, for a large part, the magnitude of predicted torque and thrust for the propeller. Of secondary importance is the solution near the 'hub' (at small radii), since its influence on induced losses is in general very small; hence other factors than induced loss minimalisation (i.e. from structural or inlet flow considerations) tend to compromise the design in that area anyway.

Finally, another type of validation is applied in paragraph 5.4: it will consider a simple limiting case for zero flow through the cylinder (the so-called ducted wake model) surrounding infinitely many helicoidal sheets and test the computational results against its exact solution. This will then also lead to a consideration of the applicability of this model to ducted propeller theory in pararagraph 5.5.

5.2 Effects of varying the computational parameters

The numerical parameters to be varied all deal of course with the appearance of the mesh or the choice between linear or quadratic elements. We will here discuss the effects of changes in the mesh, considering linear elements only.

As was stated in the previous section, three sets of parameters determine the mesh; in transverse direction (between the vortex sheets) there is the choice of number of elements m and the size reduction factor f1. It applies globally for the inner and outer region. No expectations were held regarding the importance of varying these two parameters.

The **inner region** includes the cross section of the vortex sheet, the solution on which we are interested in. High accuracy is required for x=0.5 onwards to x=1.0. A relatively high number of elements, possibly combined with a refinement near the tip (x=1.0) is expected to yield the better results. Also, the lower

boundary, corresponding to the cut-out because of the singularity at x=0, needs to be chosen. A typical value of 0.01 will do as a starting point, but repeated calculations in several ranges of advance coefficient are necessary to become confident of an appropriate value. The final solution should not be too sensitive towards small changes around this value.

In this context it is worthwile to mention that it is possible to deliberately take a larger value for the lower boundary, representing the effect a hub can be modelled to have on the optimum circulation distribution; it is appropriate to consider this as a 'virtual hub'. Mc Cormick (ref.7) is an instance of an engineer adopting this approach. It can be observed that the circulation at the inner station increases (strongly) when increasing the virtual hub diameter.

The **outer region** is special in the sense that it represents the outer flow and is surrounded by three sides on which a zero boundary condition applies. Therefore, the magnitude of the solution will be very low, except possibly for the element in the transverse zone near the tip. Because of the same reasons the influence of the choice for the upper limit (representing infinity) can be expected to be very small indeed; the choice will typically be in the order of 1.5 or 2.0, where moreover a relatively small number of elements will suffice.

The different solutions were judged from observing both the (linear) contourplot and graphs of the solution along the sheet. To indicate which specific settings of parameters are used, we will in the following use the notation:

[n_i, f1; n_o, f2] [x_low, x_upp] ([m,f3])

to mean that n_i inner elements (refinement f1) were applied with n_o outer elements (refinement f2), with a computational domain extending from x_low to x_upp (same for m and f3 in y-direction (optional)).

At the 'standard conditions' established in the previous paragraph a combination of [10,0.3; 4,10.0][.01,2.0] both the maximum value attained and the contourplot were found to be little affected by the number m (10 or 20) of elements in the y-direction. It was therefore set equal to [10,0.25] for relatively accurate solutions.

A typical example of the influence of the element distribution along the sheet was demonstrated. The maximum value along the sheet was reproduced with high accuracy regardless whether 20 or 30 inner elements were used or the refinement was 1.0 or 0.3. As was to be expected, the inflection area at small radii (where the solution is of minor importance) showed a discrepancy for f1=0.3, but this soon vanished at larger radii and was almost absent for [20,1.0], i.e. no reduction in size.

5.3 Comparison of results for different advance coefficients

Based on the data given in the references mentioned in paragraph 5.1, three comparisons are made that should give an impression of the method's accuracy over the range of advance coefficients encountered in practice. This range can be devided into three categories for the velocity ratio:

low : 0.2
medium: 0.5
high : 1.0.

The computations are all performed assuming a 2 bladed propeller and linear elements, while the computational lower bound is kept at 0.01.

For the low advance coefficient, typical of low speed applications, figure 13 compares the original data from Goldstein (also shown in fig.8) to the finite element result using 20 linear elements. The result is deemed satisfactory. The discrepancy at the root gradually disappeared when the local element size was reduced, but this implies that less points are available in the more important middle and tip area. However, this coarser grid at the tip did not seem to influence the curve itself very much; it just involves a suitable fitting routine to fill in the missing parts. This behaviour is also demonstrated in the next case.

At intermediate velocity ratio (0.5), both the calculated magnitude and the shape compare very well (fig.14) to Kramer's data presented by Theodorsen. As in the previous case, the solution in the inner region improves when no element

refinement is applied at the tip (equal number of elements), while no or little loss of accuracy occurs for this tip region.

A similar comparison can be seen in figure 15 for high advance ratio. The discrepancy with Kramer is slightly bigger here, which cannot be conclusively ascribed as a shortcoming ot either of these methods.

Formally, Goldstein's method of solution is not completely exact, since it does not guarantee the continuity (first and second order) of the solutions he obtained for the inner and outer region separately (each being treated in a different way). If a noticable deviation of the exact solution would occur, then this would happen at high advance coefficients. Also, Kramer obtained his results by interpolation techniques, which can be a potential source of error. Theodorsen therefore stresses the fact that optimum circulation distributions for high advance coefficient have been obtained by (his) electrical analogy measurements only. It has in this report been demonstrated that the finite element method offers an alternative.

5.4 Comparison to results from infinite number of blades

For the limiting case of an infinite number of blades, the circulation at a radius r can be found by means of a simple integration along the circumference, where the tangential component of the velocity is constant. It must then be assumed that the (induced) velocity is everywhere **normal** to the (imaginary) sheets in the wake, an assumption corresponding to the approach in paragraph 2.2, where only the component of the solution normal to the sheet was effectively considered by putting the partial derivatives in the direction along the sheet equal to zero.

Thus the circulation for the homogeneous tangential velocity component becomes (fig.3):

$$\Gamma(r) = 2\pi\, r\, w.\cos\psi.\sin\psi \qquad (5.3)$$

Now, using (5.1), the circulation coefficient can easily be found to yield:

$$K(r)^{\infty} = \cos^2\psi \qquad (5.3)$$

where ψ is the local pitch angle (at radius r) in the wake.

In order to use this as a comparison case, a modification was made to the boundary conditions, taking into account the fact that for an infinite number of blades there will be no in- and outflow from the inner region towards the outer region. This corresponds to locating the outer boundary (fig.4) at radius R, which means that $\partial\Omega_3$ is divided into two parts: a Neumann boundary condition of zero flow must be specified for r=R. At this point the equivalent model that we thus have created in three dimensions, corresponds to a system of axially translating vortex sheets as before, but this time moving within a rigid cylinder of the same diameter.

This is also a model, applicable to the wake of a ducted propeller. Applying these boundary conditions, one would expect that the solution for an arbitrary number of blades corresponds to the circulation around the blades of an upstream propeller operating in a duct. This subject will be pursued further in the next paragraph on a preliminary basis; in anticipation we will tentatively adopt the name 'ducted wake' for this model.

In this configuration, even a modest number of blades should for relatively low advance ratio yield results not far removed from the solution for the infinitely bladed open propeller as given by (5.3). This was illustrated by computing the solution for the low velocity ratio (0.2) case from the previous paragraph, combined with a 4-bladed 'ducted propeller'. The results are illustrated in figure 16, where the computed points can be seen to lie particularly close to the solid curve.

5.5 Tentative results for ducted propeller

As was illustrated in the previous paragraph, the circulation distribution for a 'ducted wake' can easily be computed. Whether this can be used to compute the equivalent circulation distribution for a (heavily loaded) ducted propeller however, is a matter that remains yet to be investigated.

The notion of a ducted propeller wake consisting of helicoidal vortex sheets surrounded by an impenetrable cylinder can be found in the work of Gray and Wright (refs. 8 & 9), who model this cylinder to emerge from the duct trailing edge, consisting of a distributed vorticity having its origin in the tip vortices from the propeller blades as they spread against the duct inner surface. The boundary conditions they apply to their computational method of singularities imply the existence of a final wake velocity component in the direction of the sheet; in other words: in their model there is no normality in the wake.

This condition emerges in the theory of Gray&Wright from an (implicitly made) assumption concerning the pitch angle of the vorticity distribution at the sheet/cylinder intersection: it is taken to be directly deducable from the magnitude of the induced velocity in the vortex cylinder, which is correctly shown to possess a certain magnitude. The next step however, from this absolute velocity to an allegedly corresponding direction, is not explicitly justified. Instead, it is implicitly taken to logically follow from the velocity diagram. Exactly this interpretation of the velocity triangle in this model will be a subject of further research.

There is at least some justification to support this interpretation however, because the resulting velocity component along the sheet (at radius R) corresponds to results obtained by the author from a momentum consideration for an infinite number of blades, applied to a (ducted) propeller wake which is cylindrical over its entire length. The results of this momentum theory are preliminary and should result in a report on the subject in the near future.

Given the assumption that there is no normality in the ultimate ducted wake, there should thus exist a potential flow solution allowing also a velocity component in the longitudinal (n-)direction. Since parallel flow is a solution that satisfies the boundary condition that the helicoidal sheets remain undisturbed, this solution can be superimposed on the solution obtained by the present method, which regards exclusively the part of the potential having a zero derivative in the longitudinal direction (see par.(2.2)). The exact superposition would necessitate the use of a method like the one used by Gray

and Wright, thereby making the solution dependent on the propeller loading. Future work will continue in this direction.

It should be stressed that the boundary conditions as suggested by Gray&Wright imply that the solution then also becomes dependent on the **loading** of the ducted propeller, i.e. it is not exclusively dependent on the geometry of the final wake.

The results acquired when normality in the wake is assumed ('ducted wake') are tentatively presented here. They are probably representative for the lightly loaded ducted propeller, where the distinction with the non-normality wake disappears. Figure 17 shows how the solution varies as more blades are considered (B=2,4,16). The velocity ratio chosen (1.365) is one that makes comparisons to the work of Gray&Wright (ref.9) possible (at which point it can be mentioned that the solutions did not correspond exactly, though light (zero) loading was assumed).

Again, for a number of blades as large as sixteen, the solution virtually coincides with the solution for an infinitely bladed open propeller, given by (5.3). Calculations, performed for even more 'blades' (99) showed this trend to continue.

The typical characteristic for this type of ducted wake solution is obviously, as was expected, the monotonous increase of the circulation towards the tip; this compares to the previous results for the open propeller where the lift gradually vanishes towards the tips. This behaviour reflects the fact that in theory the ducted propeller blade can be thought to end at the duct surface, leaving zero gap. A non-zero gap could however be programmed by way of including this leak flow through the gap which of course will almost allways occur in practice.

SECTION 6

CONCLUSIONS

A dedicated finite element application has been developed to find a solution for an apparently three dimensional Laplace problem (potential flow) that appears in the context of propeller design. No special difficulties have been encountered in the translation to a finite element formulation.

The classical tables provided by Goldstein, Lock and Kramer have been confirmed on a sampling basis with acceptable accuracy; this may be taken to indicate that both their results and the present program are correct.

In doing so it has been demonstrated that the program provides an easy and flexible method of finding circulation distributions for arbitrary number of blades and arbitrary advance ratio.

The method could easily be adapted to model a ducted propeller wake. However, the presently used boundary conditions only determine the solution normal to the 'vortex sheets'; therefore the solution **along** the sheets is not considered, which is quite valid for an open propeller. For the solution of the heavily loaded ducted propeller this direction should be considered as well. Thus, the 'ducted wake' solution obtained, applies exclusively to light loading, where the distinction between the two approaches vanishes.

A number of linear elements which is not excessive (8x20 inner elements) yields satisfactory results, in particular the important maximum circulation is calculated with a small error even for a small number of elements (10).

In both developing and using the program the programmer's and (interactive) user environment of Prospero Fortran (supporting GEM) on an Atari 1040 ST computer proved stimulating contributions to this work.

LIST OF TABLES

table 9.

B=2, lambda=1.0

FEM, [20,0.3; 4,10.0]

[10,0.25][0.01,2.0]

LIST OF FIGURES

15 Comparison to Kramer's results for high advance coefficient ($B=2$, $\lambda_3=1.0$).

16 Ducted wake solution, comparison to open propeller with infinite number of blades at low advance coefficient.

17 Ducted wake results for increasing numbers of blades at high advance coefficient and comparison to infinite blade solution.

REFERENCES

1 S. Goldstein
"On the Vortex Theory of Screw Propellers"
Proc. Roy. Soc., Series A, Volume 123, 1929

2 C.N.H. Lock, R.C. Panckhurst
"Strip Theory Method of Calculation for Airscrews on High Speed Aeroplanes"
R and M 2035, 1945

3 A.J. Bocci, J.I. Morrison
"A Review of ARA Research into Propeller Aerodynamic Prediction Methods"
AGARD Conference Proceedings No.366: Aerodynamics and Acoustics
of Propellers, 1984

4 T. Theodorsen
"Theory of Propellers"
McGraw-Hill, 1948

5 K.N. Kramer
"The Induced Efficiency of Optimum Propellers Having a Finite Number of Blades"
NACA Tech. Mem., 884, 1939

6 R.M. Bass
"Propeller Performance Prediction and Design Techniques"
VKI Lecture Series 1982-08, 1982

7 B.W. McCormick jr.
"Aerodynamics of V/STOL Flight"
Academic Press, 1967

8 R.B. Gray and T. Wright
"A Vortex Wake Model for Optimum Heavily Loaded Ducted Fans
(AIAA paper 69-222, Atlanta, Ga, 1969
J. Aircraft March-April 1970 vol. 7, no. 2

9 T. Wright
"Evaluation of the design parameters for Optimum Heavily Loaded Ducted Fans"
J. Aircraft November-December 1970 vol. 7 no. 6.

table 1.
B=4, lambda=0.2
(Lock&Yeatman)

x	K(x)
0.1	0.300
0.2	0.506
0.3	0.706
0.4	0.786
0.5	0.848
0.56	0.871
0.6	0.881
0.7	0.887
0.76	0.872
0.8	0.850
0.9	0.714
0.96	0.503
1.0	0.554

table 2.
B=4, lambda=0.5
(Lock&Yeatman)

x	K(x)
0.1	0.064
0.2	0.173
0.3	0.283
0.4	0.377
0.5	0.449
0.6	0.492
0.7	0.501
0.8	0.469
0.9	0.370
1.0	0.000

table 3.
B=2, lambda=0.2
(Goldstein)

x	K(x)
0.04	0.124
0.08	0.240
0.12	0.344
0.16	0.434
0.20	0.511
0.24	0.575
0.28	0.626
0.32	0.669
0.36	0.704
0.40	0.731
0.50	0.770
0.60	0.775
0.70	0.747
0.80	0.671
0.90	0.519
0.96	0.351
1.00	0

table 4.
B=2, lambda=0.5
(Goldstein)

x	K(x)
0.1	0.092
0.2	0.175
0.3	0.243
0.4	0.295
0.5	0.329
0.6	0.341
0.7	0.331
0.8	0.295
0.9	0.220
1.0	0

table 5.
B=2, lambda=0.5
(Kramer)

x	K(x)
0.1	0.0919
0.2	0.1758
0.3	0.246
0.4	0.297
0.5	0.331
0.6	0.345
0.7	0.338
0.75	0.325
0.8	0.305
0.85	0.276
0.9	0.235
0.95	0.173
1.0	0

table 6.
B=2, lambda=1.0
(Kramer)

x	K(x)
0.1	0.0283
0.2	0.0552
0.3	0.0795
0.4	0.0999
0.45	0.1082
0.5	0.1155
0.6	0.1239
0.7	0.1243
0.75	0.1213
0.80	0.1156
0.85	0.1061
0.90	0.0919
0.925	0.0817
0.95	0.0687
0.975	0.0497
1.0	0

table 7.
B=4, lambda=0.2
FEM, [20,0.3; 4,10.0]
[10,0.25][0.01,2.0]

x	K(x)
0.0100	0.0254
0.0946	0.1032
0.1746	0.3758
0.2486	0.5544
0.3185	0.6720
0.3842	0.7502
0.4458	0.8030
0.5037	0.8388
0.5580	0.8629
0.6090	0.8780
0.6568	0.8854
0.7017	0.8853
0.7438	0.8774
0.7834	0.8603
0.8205	0.8322
0.8554	0.7905
0.8881	0.7315
0.9188	0.6497
0.9476	0.5349
0.9746	0.3615
1.0000	0

table 8.
B=2, lambda=0.5
FEM, [20,0.3; 8,10.0]
[10,0.25][0.01,2.0]

x	K(x)
0.0100	0.0116
0.0946	0.0512
0.1746	0.1279
0.2486	0.1887
0.3185	0.2373
0.3842	0.2751
0.4458	0.3035
0.5037	0.3237
0.5580	0.3366
0.6090	0.3431
0.6568	0.3438
0.7017	0.3394
0.7438	0.3301
0.7834	0.3163
0.8205	0.2980
0.8554	0.2750
0.8881	0.2467
0.9188	0.2116
0.9476	0.1665
0.9746	0.1033
1.0000	0

table 9.
B=2, lambda=1.0
FEM, [20,0.3; 4,10.0]
[10,0.25][0.01,2.0]

x	K(x)
0.0100	0.0036
0.0946	0.0163
0.1746	0.0410
0.2486	0.0613
0.3185	0.0783
0.3842	0.0923
0.4458	0.1035
0.5037	0.1121
0.5580	0.1181
0.6090	0.1219
0.6568	0.1235
0.7017	0.1231
0.7438	0.1207
0.7834	0.1164
0.8205	0.1102
0.8554	0.1019
0.8881	0.0913
0.9188	0.0777
0.9476	0.0599
0.9746	0.0355
1.0000	0

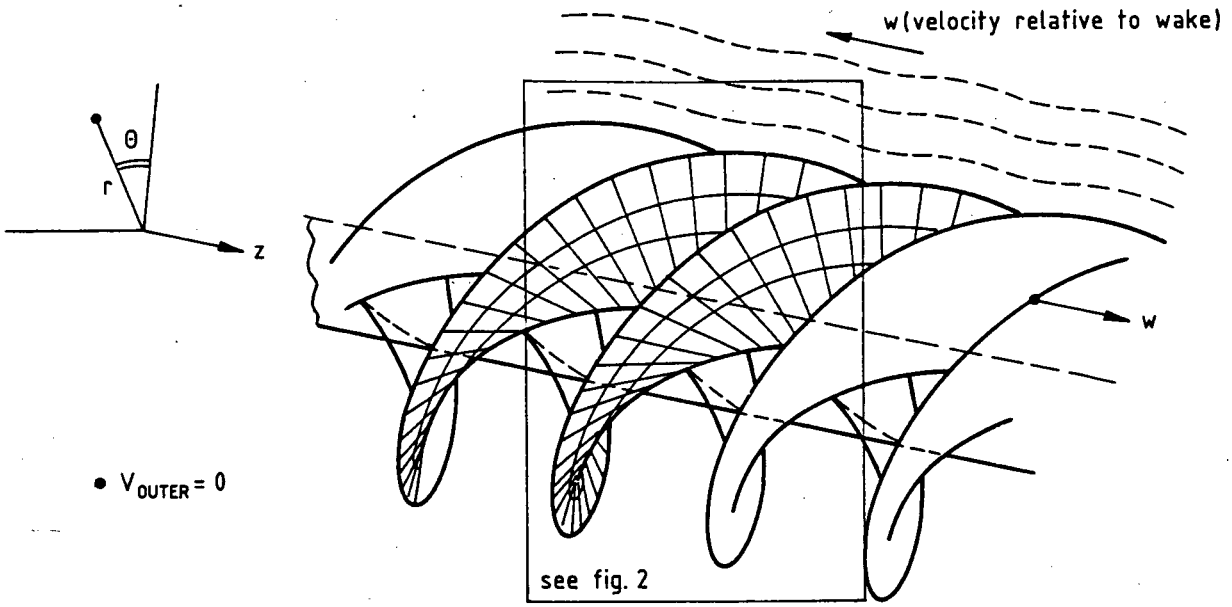

Figure 1: A system of helicoidal vortex sheets.

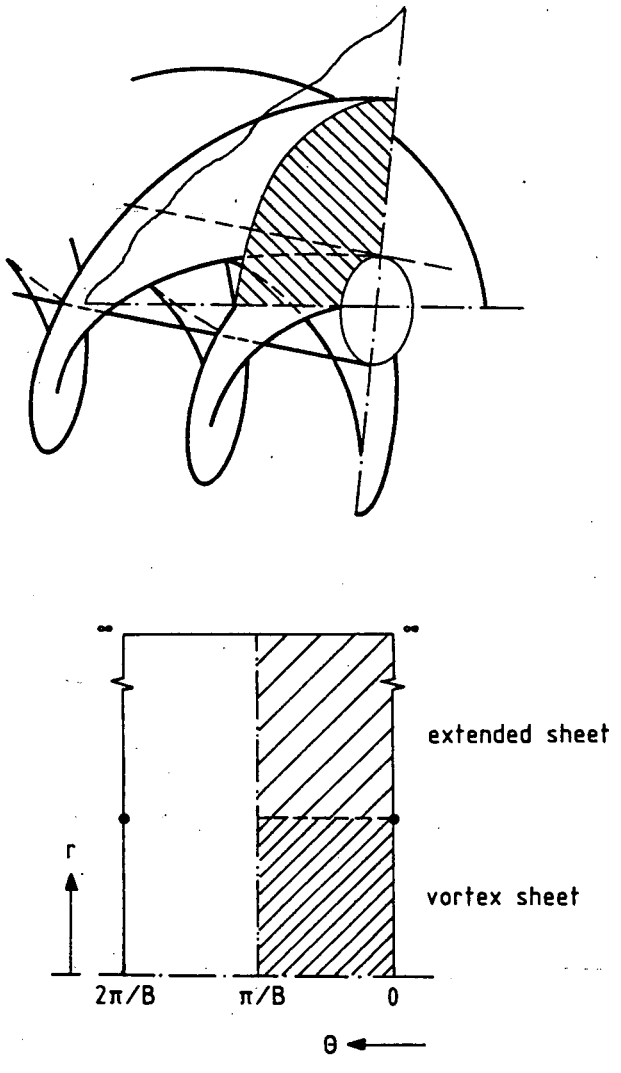

Figure 2: Elementary "unit cell" indicating computational domain.

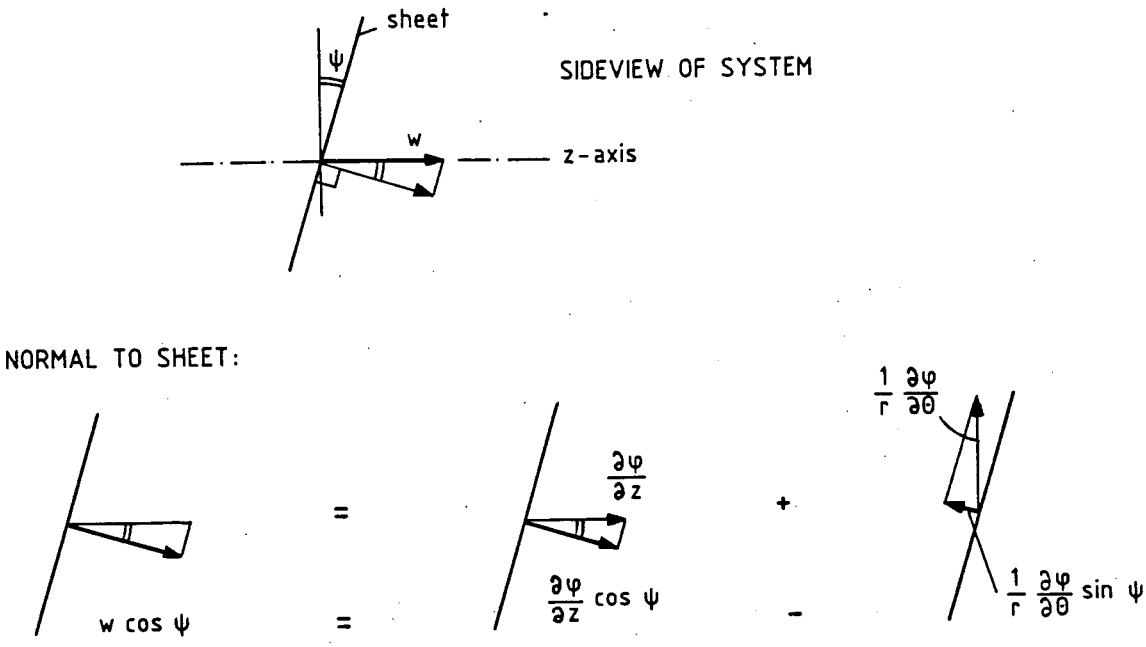

Figure 3: Boundary conditions for the vortex sheet.

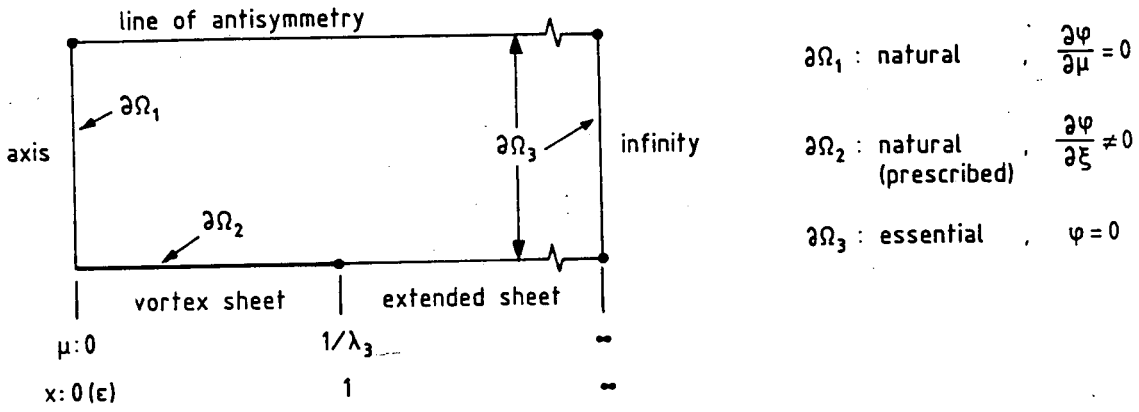

Figure 4: Computational domain and boundary conditions.

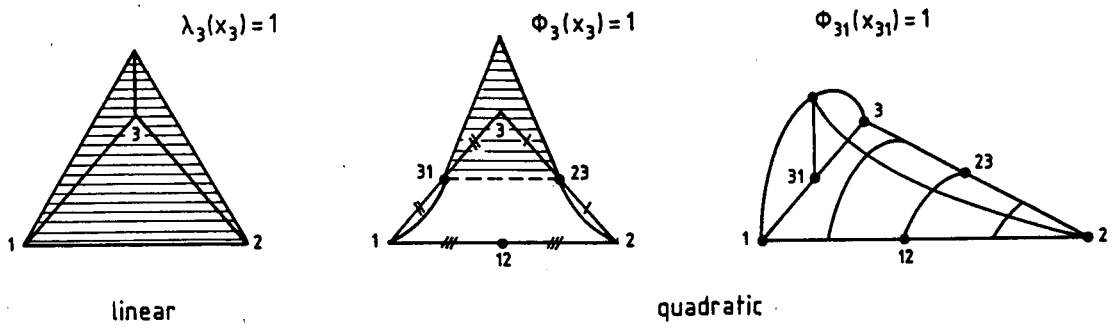

Figure 5 : The linear and quadratic support functions on a triangular element.

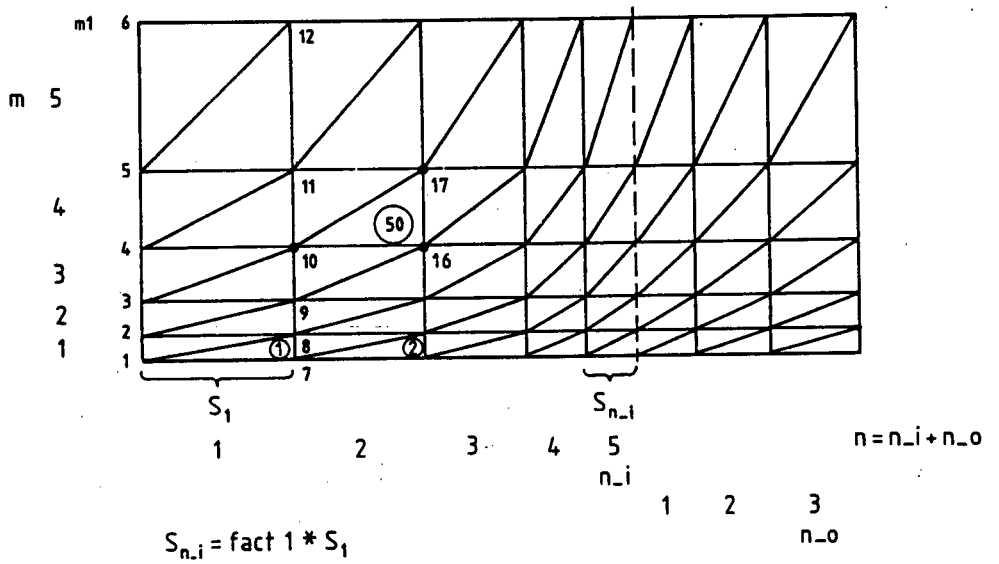

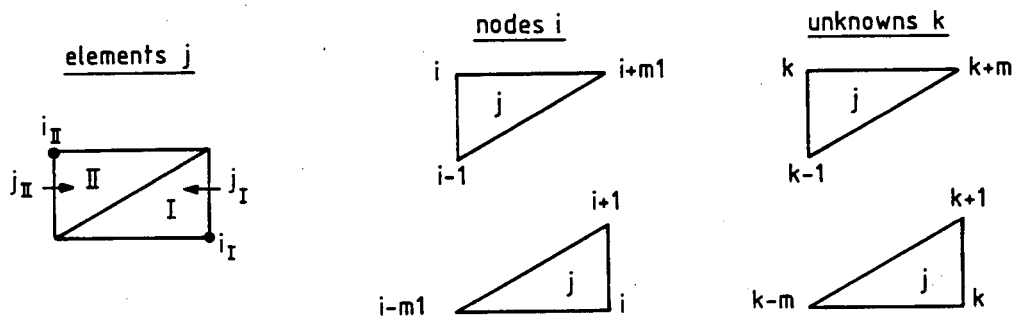

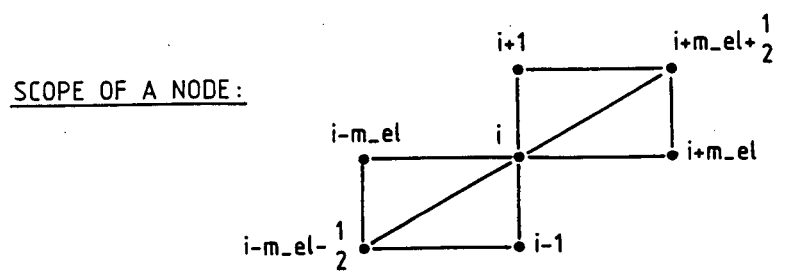

Figure 6 : The numerical mesh (linear elements).

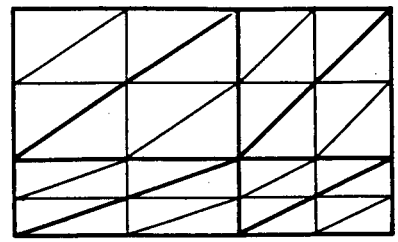

Figure 7 : Quadratic mesh retraining topology of Fig. 6.

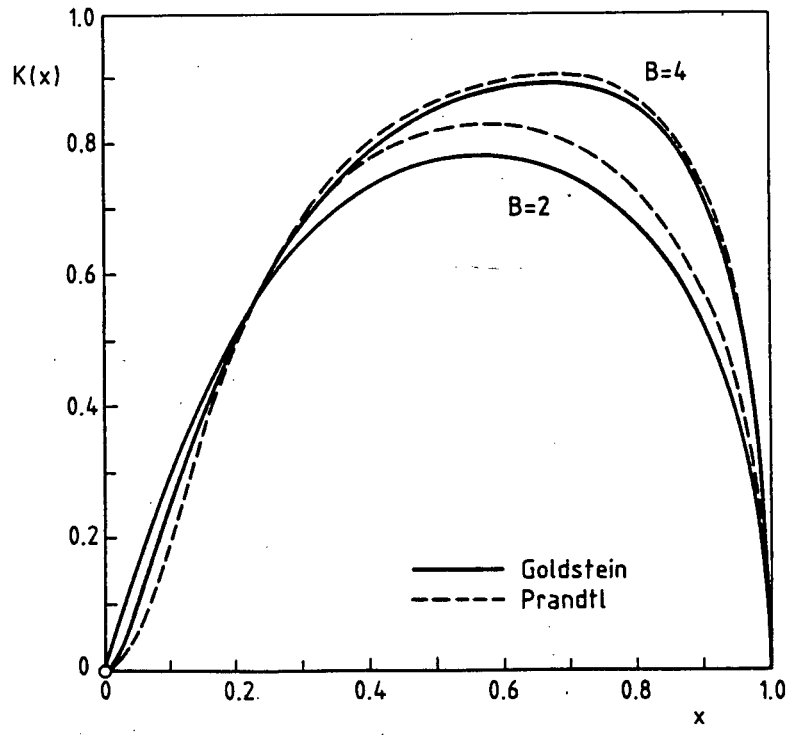

Figure 8 : Solution for B=2 and B=4 at low advance ratio ($\lambda_3 = 0.2$) according to Goldstein.

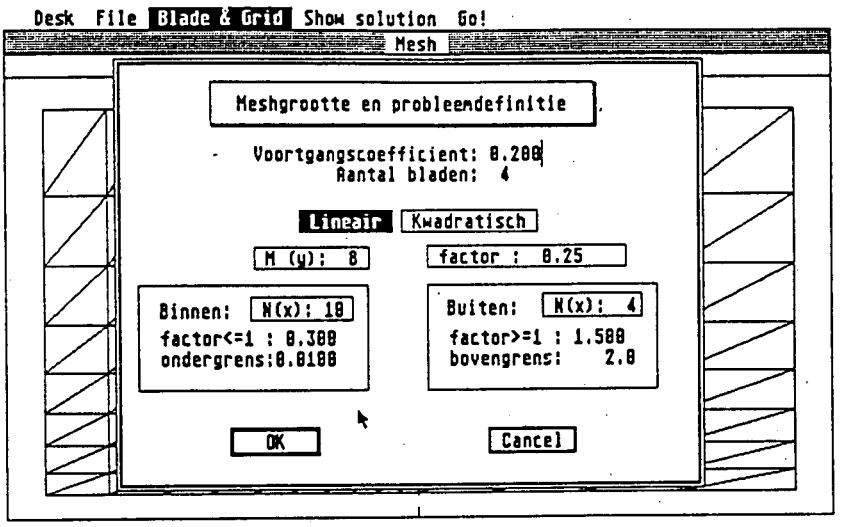

Figure 9 : Problem definition and mesh specification in a "dialogbox".

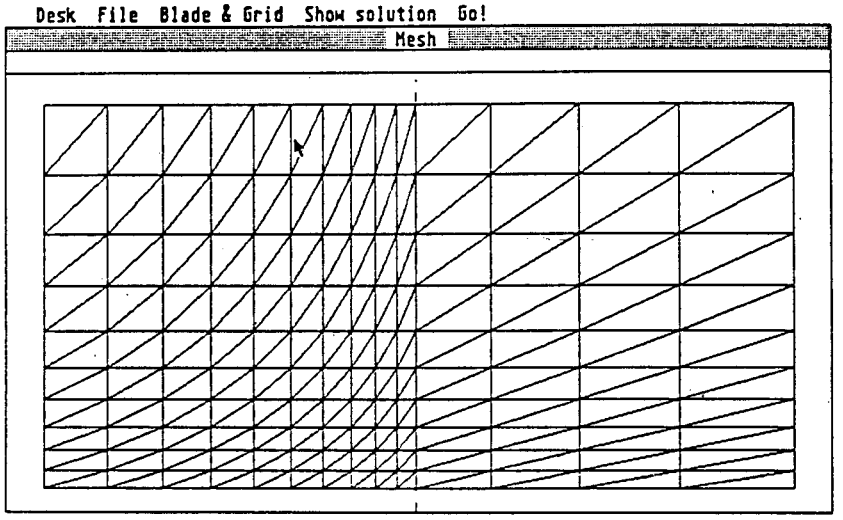

Figure 10 : Visual inspection of the mesh.

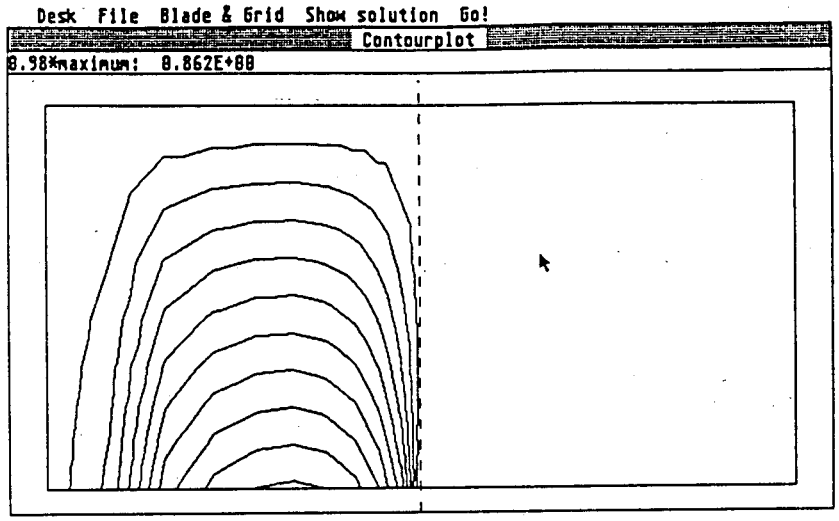

a)

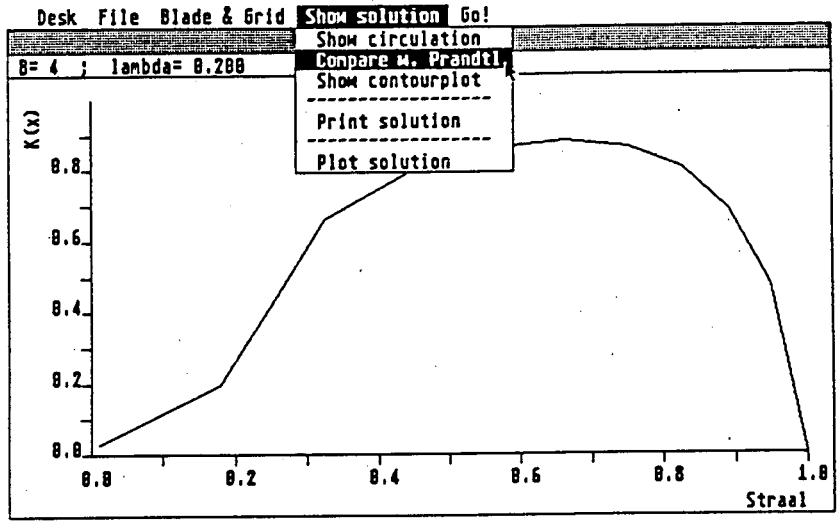

b)

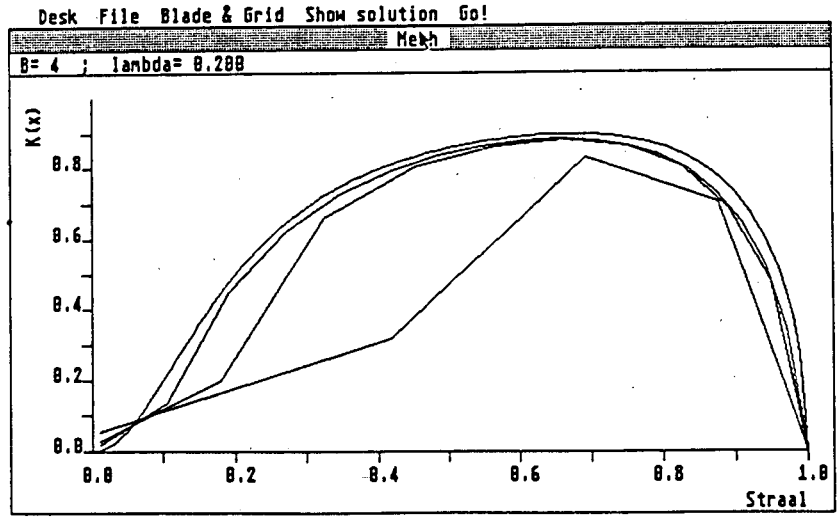

c)

Figure 11 : Several possibilities of inspection of the solution : contourplot or circulation along the radius ($B=4$, $\lambda_3=0.2$).

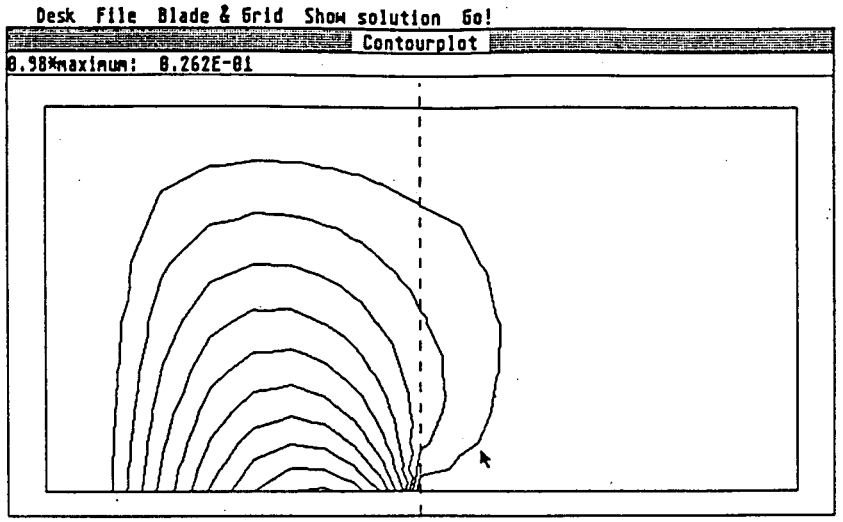

Figure 12 : Contourplot of solution for high advance ratio ($B=4, \lambda_3=3.0$) showing pronounced in/out-flow features.

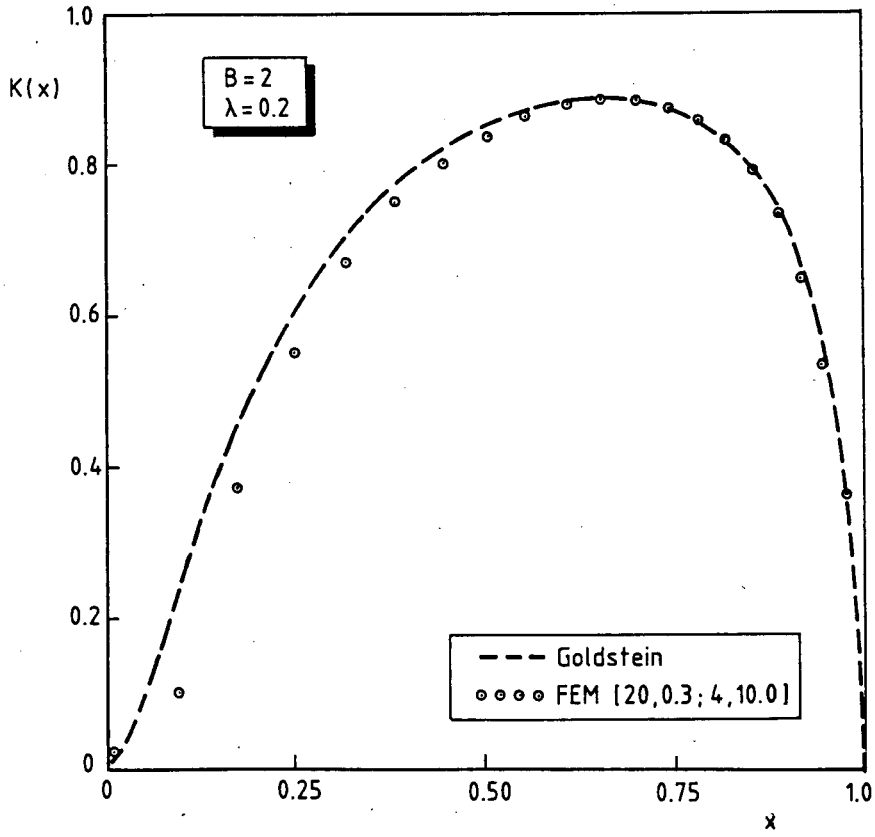

Figure 13 : Comparison of Goldstein's solution (dashed) to FEM results for 20 inner elements (low advance coefficient).

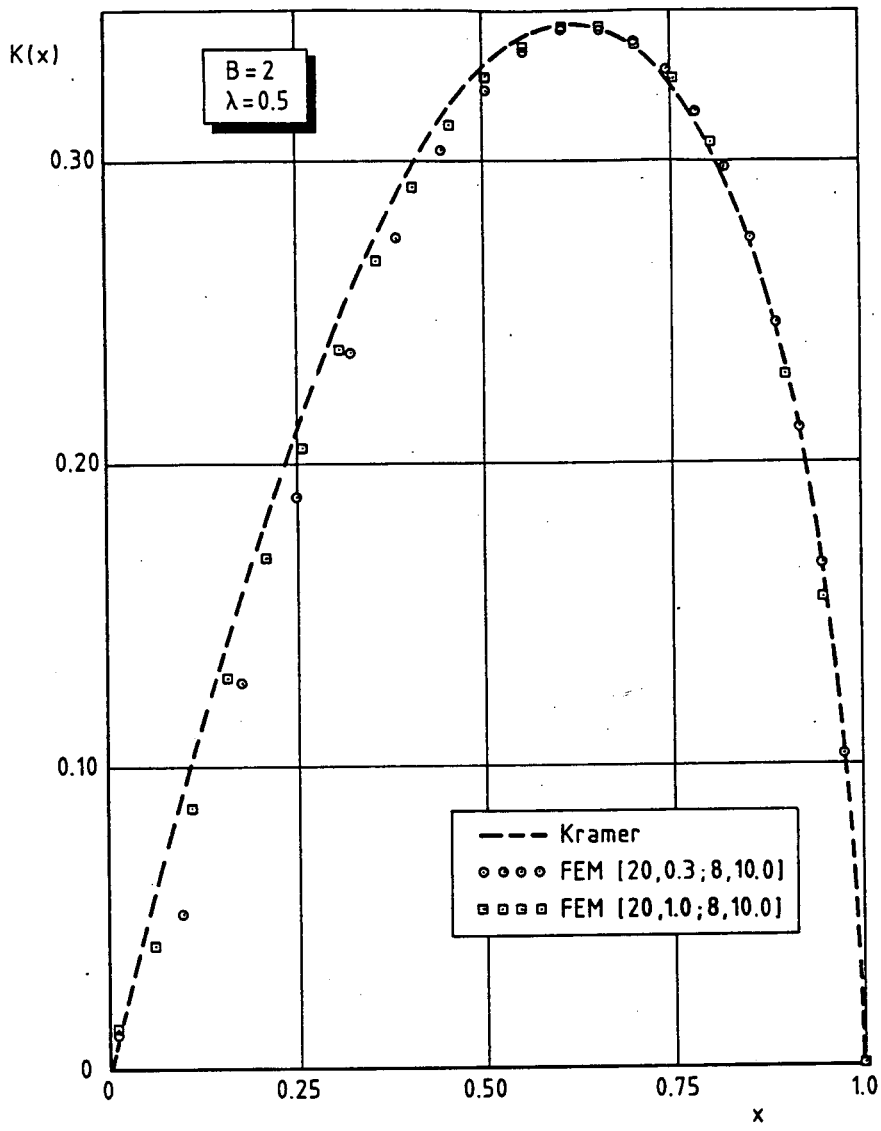

Figure 14 : Comparison of Kramer and FEM results for intermediate advance coefficient.

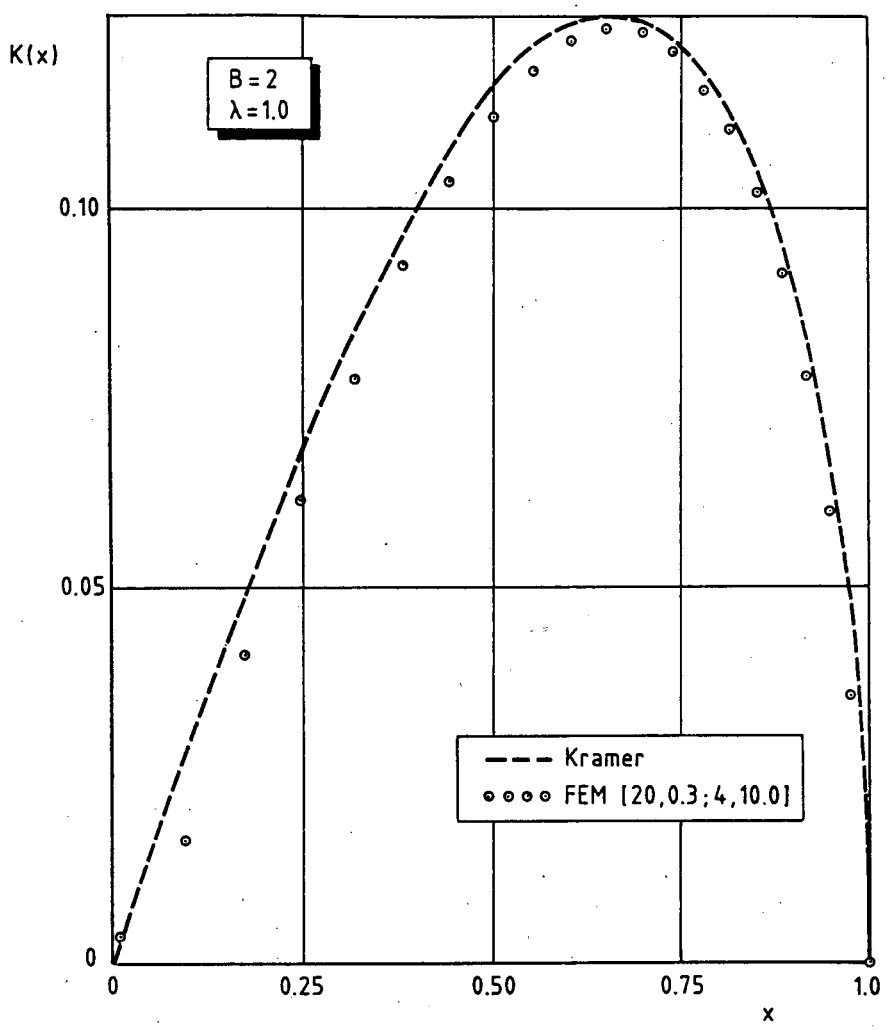

Figure 15 : Comparison to Kramer's results for high advance coefficient.

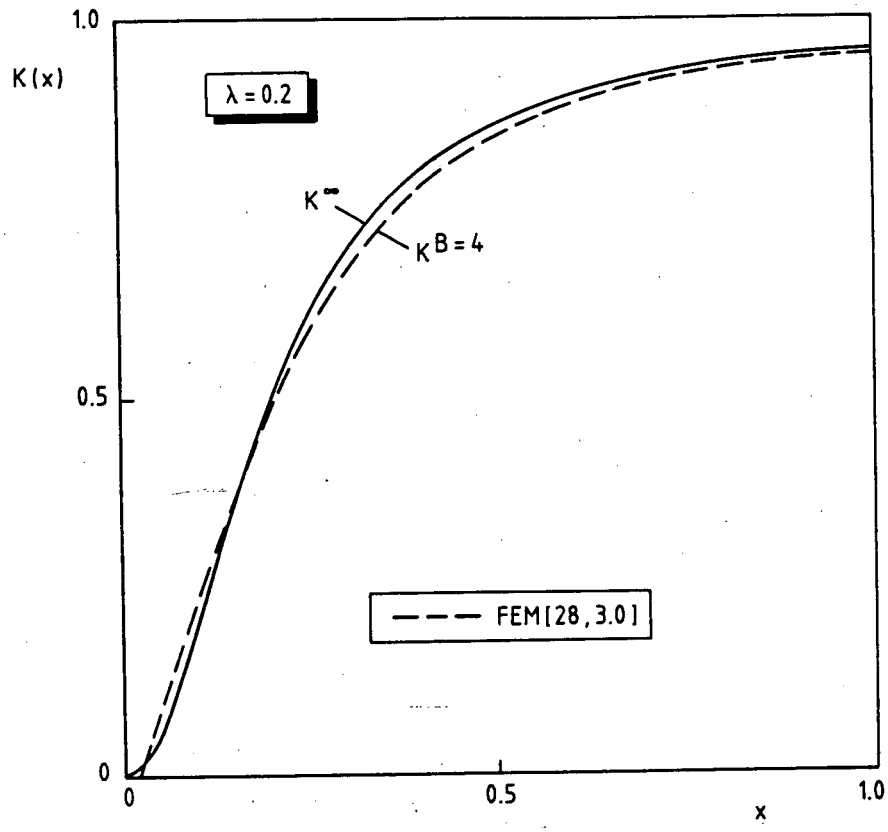

Figure 16 : Ducted wake solution, comparison to open propeller with infinite number of blades.

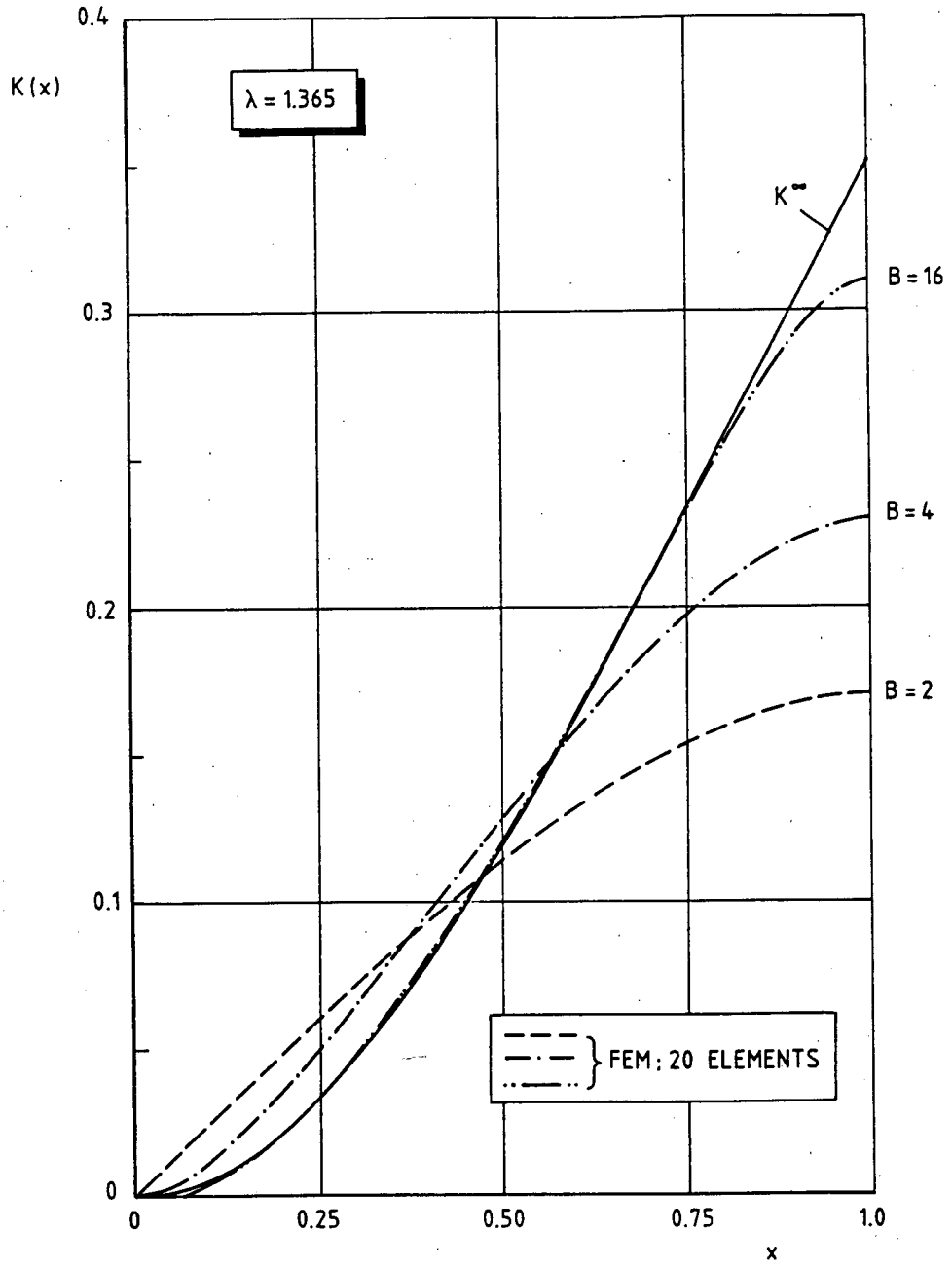

Figure 17: Ducted wake results for increasing number of blades, and comparison to infinite blade solution.